THE JOURNAL OF BIOLOGICAL CHEMISTRY
Vol. 275, No. 34, Issue of August 25, pp. 26265–26276, 2000
Printed in U.S.A.

Molecular Recognition of Taxol by Microtubules

KINETICS AND THERMODYNAMICS OF BINDING OF FLUORESCENT TAXOL DERIVATIVES TO AN EXPOSED SITE*

Received for publication, April 12, 2000, and in revised form, May 11, 2000
Published, JBC Papers in Press, May 18, 2000, DOI 10.1074/jbc.M003120200

J. Fernando Díaz‡§, Rik Strobe¶, Yves Engelborghs¶, André A. Souto‖, and José M. Andreu‡**

From the ‡Centro de Investigaciones Biológicas, Consejo Superior de Investigaciones Científicas, C/Velázquez, 144, 28006 Madrid, Spain, the ¶Laboratory of Biomolecular Dynamics, Katholieke Universiteit Leuven, Celestijnenlaan 200D, B-3001 Heverlee, Belgium, and ‖Instituto de Química Orgánica, Consejo Superior de Investigaciones Científicas, C/Juan de la Cierva 3, 28006 Madrid, Spain

We have determined the kinetic scheme and the reaction rates of binding to microtubules of two fluorescent taxoids, 7-*O*-[*N*-(4′-fluoresceincarbonyl)-L-alanyl]Taxol (Flutax-1) and 7-*O*-[*N*-(2,7-difluoro-4′-fluoresceincarbonyl)-L-alanyl]Taxol (Flutax-2). Flutax-1 and Flutax-2 bind to microtubules with high affinity ($K_a \approx 10^7$ M^{-1}, 37 °C). The binding mechanism consists of a fast bimolecular reaction followed by at least two monomolecular rearrangements, which were characterized with stopped-flow techniques. The kinetic constants of the bimolecular reaction were $6.10 \pm 0.22 \times 10^5$ M^{-1} s^{-1} and $13.8 \pm 1.8 \times 10^5$ M^{-1} s^{-1} at 37 °C, respectively. A second slow binding step has been measured employing the change of fluorescence anisotropy of the probe. The reversal of this reaction is the rate-limiting step of dissociation. A third step has been detected using small angle x-ray scattering and involves a 2-nm increase in the diameter of microtubules. It is suggested that the first step entails the binding of the Taxol moiety and the second a relative immobilization of the fluorescent probe. The equilibrium and some kinetic measurements required the use of stabilized cross-linked microtubules, which preserved taxoid binding. The results indicate that the Taxol binding site is directly accessible, in contrast with its location at lumen in the current model of microtubules. An alternative structural model is considered in which the binding site is located between protofilaments, accessible from the microtubule surface.

Microtubules are polymers assembled from $\alpha\beta$-tubulin heterodimers. Among other functions, they form the mitotic spindle, which segregates the chromosomes during cell division. Due to this function, they are the target of antimitotic drugs like *Vinca* alkaloids and taxoids, used in cancer treatment (1, 2). Taxol[1] is extensively employed in therapy of ovarian cancer, metastatic breast cancer, head and neck cancer, and lung cancer (3–5). Taxol arrests cell division by blocking microtubule dynamics, which is necessary for their function (6). These dynamics are normally controlled by the nucleotide content of tubulin; the heterodimer binds two molecules of guanine nucleotide: a nonexchangeable GTP molecule at the α-subunit, which plays a structural stability role (7), and a second exchangeable molecule bound to the β-subunit, which can be either GTP or GDP. This second nucleotide molecule controls the activation state of the protein. In the GDP-bound state, the protein is in an inactive conformation, forming double rings (8), whereas in the GTP state it is active for microtubule assembly. GTP hydrolysis in the polymers and GDP/GTP exchange in the dimers control the assembled state of tubulin (9).

Taxol drives inactive GDP-tubulin into microtubules, replacing the need of the γ-phosphate of GTP to activate the protein (10). It was the first microtubule assembly-promoting drug to be discovered (11). Taxol stabilizes microtubules by binding preferentially to assembled purified tubulin with an exact 1:1 stoichiometry (10). Thus, the cellular microtubule cytoskeleton should have a very large number of binding sites for Taxol or other endogenous ligands, whose function is unknown. Unassembled tubulin shows insignificant affinity for Taxol (12–14), indicating that the binding site is mostly formed by the polymerization process. The interaction of microtubules with Taxol has been widely studied (10, 12–25). However, since Taxol binding and microtubule assembly are linked reactions and the binding affinity seems to be high (12, 14), direct measurements of the binding thermodynamics are extremely difficult. In addition, the coincidence of the protein and Taxol absorption bands has precluded, up to now, the use of spectroscopic techniques to study the kinetics of the reaction.

Taxoid binding affects the microtubular structure (26, 27). In a previous study (23), kinetic measurements of the interchange of radioactive labeled Taxol and docetaxel showed that taxoids are able to bind and dissociate freely from microtubules in less than 3 min. The same work demonstrated that the addition of Taxol to preformed microtubules made of pure tubulin alters their structure in less than 2 min. Those results indicate that the taxoid binding site is accessible in the microtubules. This is supported by the rapid Taxol-induced increase of flexibility of assembled microtubules (28) and by the fast binding and dissociation of 7-*O*-[*N*-(4′-fluoresceincarbonyl)-L-alanyl]Taxol (Flutax-1) to cellular microtubules (24). All of these characteristics would be compatible with a taxoid binding site in a zone

* This work was supported by Comunidad Autonoma de Madrid Grant 07B/0025/99, Dirección General de Enseñanza Superior e Investigación Científica (DGESIC) Grants PB-95-0116 and APC 96-0071, and Fundación Científica de la Asociación Española contra el Cancer (to J. M. A.) and DGESIC Grant PB-96-0852 (to U. Acuna). The costs of publication of this article were defrayed in part by the payment of page charges. This article must therefore be hereby marked "*advertisement*" in accordance with 18 U.S.C. Section 1734 solely to indicate this fact.

§ To whom correspondence should be addressed. Tel.: 34-915611800 (ext. 4380); Fax: 34-915627518; E-mail: fer@akilonia.cib.csic.es.

** Present address: Faculdade de Quimica, Universidade Pontificia Catolica do Rio Grande do Sul, 90619-900, Porto Alegre-RS, Brasil.

[1] The abbreviations and trivial names used are: Taxol® (Bristol-Myers Squibb) (paclitaxel), 4,10-diacetoxy-2α-(benzoyloxy)-5β,20-epoxy-1,7β-dihydroxy-9-oxotax-11-en-13α-yl(2R, 3S)-3-[(phenylcarbonyl) amino]-2-hydroxy-3-phenylpropionate; docetaxel (Taxotere®; Rhône-Poulenc Rorer RP56976), 4-acetoxy-2α-(benzoyloxy)-5β,20-epoxy-1,7β,10β-trihydroxy-9-oxotax-11-en-13α-yl(2*R*,3*S*)-3-[(tert-butoxycarbonyl)amino]-2-hydroxy-3-phenylpropionate.

between the protofilaments (20, 26, 27, 29). However, in the model structure of Taxol stabilized microtubules (obtained by fitting into an electron microscopy density map (30) the biochemically well supported (31–33) high resolution model of the tubulin-Taxol complex (34)), the Taxol binding site is at one side of the β-tubulin subunit, clearly facing the microtubular lumen.

In order to unveil the kinetic mechanisms of molecular recognition of ligands by the Taxol binding site of microtubules, we have employed two taxoids labeled at position 7 of the taxane ring either with fluorescein (Flutax-1; Refs. 24 and 35) or difluorofluorescein (7-*O*-[*N*-(2, 7-difluoro-4′-fluoresceincarbonyl)-L-alanyl]Taxol; Flutax-2). The use of these probes, which retain the microtubule assembly activity, has allowed a detailed kinetic characterization of the reversible interaction of microtubules and taxoids. The results evidence an amazingly fast initial binding reaction and provide further insight into the interaction of microtubules with Taxol.

EXPERIMENTAL PROCEDURES

Tubulin, Microtubules, and Taxoids—Purified calf brain tubulin and chemicals were as described (27). For glycerol-induced assembly, tubulin was directly equilibrated in 10 mM phosphate, 1 mM EDTA, 0.1 mM GTP, 3.4 M glycerol, pH 6.7, buffer. All tubulin samples were clarified by centrifugation at 50,000 rpm, 4 °C, for 10 min using TL100.2 or TL100.4 rotors in a Beckman Optima TLX centrifuge. After centrifugation, 6 mM $MgCl_2$ and up to 1 mM GTP were added to the solution, final pH 6.5 (GAB). Microtubules were assembled by raising the temperature to 37 °C for 30 min. The length and morphology of the assembled microtubules were checked by negative stain electron microscopy as described (27).

Axonemes from sea urchin (*Strongylocentrotus purpuratus*) sperm tail were kindly provided by Dr. Philippe Huitorel, Université Pierre et Marie Curie Villefranche-sur-Mer, France) and diluted a minimum of 100 times in the experimental buffer.

Docetaxel was kindly provided by Rhône-Poulenc Rorer (Antony, France). Flutax-1 was synthesized as described (35). Their concentrations were measured spectrophotometrically (10, 24). Flutax-2 was synthesized by the reaction of 7-*O*-(L-alanyl) Taxol with Oregon Green 488 carboxylic acid, succinimidyl ester ("5 isomer," Molecular Probes reference no. 0–6147), following the described procedures (35), and purified by preparative TLC on silica gel with chloroform/methanol/acetic acid (4:1:0.15, v/v/v) as eluent; mass spectrum and NMR data were in accordance with its structure (58). Flutax-2 purity (high performance liquid chromatography; Ref. 24) was 94%. Flutax-2 induced the assembly of GDP-tubulin similarly to Flutax-1 (24) except for the critical tubulin concentration, which was coincident with Taxol. Flutax-2 concentrations were measured in 0.5% SDS, 50 mM sodium phosphate buffer, pH 7.0, employing an extinction coefficient[2] of 49,100 ± 1100 M^{-1} cm^{-1} at 496 nm.

Preparation of Cross-linked Microtubules—In order to stabilize microtubules against disassembly by dilution and low temperatures, 50 μM tubulin in GAB was assembled at 37 °C for 30 min, and then 20 mM glutaraldehyde (EMscope, microscopy grade) was added to the solution, which was incubated at 37 °C for 10 min more. The remains of the cross-linking agent were quenched by adding 60 mM $NaBH_4$ (Fluka) on ice and the mixture degassed. Under these conditions, 90% of the tubulin was found to be incorporated into the microtubules. The morphology of the cross-linked microtubules was checked by electron microscopy and found to be normal. They were found to be stable against dilution and low temperatures. The taxoid binding was found to be unaffected by the treatment as judged by the stoichiometry and the kinetics of the binding reaction, which were not altered. The number of active sites was found to decay at a relatively slow rate (~5% decay in 24 h at 4 °C).

Binding of Fluorescent Taxoids to Microtubules—The binding of Flutax-1 and Flutax-2 to the microtubules was measured using a centrifugation assay. Samples of cross-linked microtubules were incubated for 1 h at different temperatures and taxoid concentrations. The samples were then centrifuged for 20 min at 50,000 rpm in a TL100 rotor employing a Beckman Optima TLX ultracentrifuge. The supernatants were taken, and the pellets were resuspended in a 10 mM phosphate buffer, pH 7.0, containing 1% SDS. The pellets and supernatants were diluted 1:5 in the same buffer, and their fluorescence was measured employing a Shimadzu RF-540 spectrofluorometer (excitation wavelength 492 nm, emission wavelength 522 nm, 5-nm excitation and emission slits). The concentration of ligand in the samples was calculated using Flutax-1 and Flutax-2 spectrophotometric concentration standards.

The percentage of inactive ligand in the stock solutions was obtained by measuring the titration curves at two different concentrations of sites, 1 and 0.1 μM. The binding constant has to be the same at both concentrations of sites and can be calculated from the apparent binding constant by discounting the percentage of the inactive ligand from the total free ligand. The value fitting both curves with the same binding constant and the minimal error was calculated using a program based on the Marquardt algorithm (36). The percentages found at each experimental temperature were averaged, and the effective binding constants were calculated using the averaged values.

The binding of Flutax-1 and Flutax-2 can also be monitored by the change in ligand anisotropy. The anisotropy of the fluorescence of Flutax-1 and Flutax-2, bound and free, were measured in a SLM-8000D fluorometer, using an excitation wavelength of 470 nm and an emission wavelength of 560 nm, with 2-nm excitation and emission slits. The binding of Flutax-1 and Flutax-2 to the microtubules was measured using a ligand anisotropy assay. Samples of taxoids were incubated for 15 min at different temperatures and concentrations of cross-linked microtubules. The anisotropy of the samples were measured in a Polastar-Galaxy (BMG Labtechnologies) plate reader using the 485-P excitation filter and the 520-P emission filter. Since with this method the binding constants are determined using the free concentration of sites (total measured binding sites minus bound ligand measured), they are not influenced by the percentage of inactive ligand.

Kinetics of Binding and Dissociation of Fluorescent Taxoids to Microtubules—The kinetics of Flutax-1 and Flutax-2 binding to and dissociation from microtubules were measured by following the change of intensity of the fluorescence of the probe, employing a High-Tech Scientific SS-51 stopped-flow device equipped with a fluorescence detection system. A wavelength of 492 nm (2-nm slit) in the excitation pathway and a filter with a cut-off of 530 nm in the emission pathway were used. The dead time of the instrument was determined using the reaction of *N*-bromosuccinimide with *N*-acetyltryptophanamide (37) and was found to be ~2 ms. With these conditions, both Flutax-1 and Flutax-2 are photostable within the time of the measurement.

The kinetics of the binding of Flutax-1 and Flutax-2 to microtubules were also measured by the change in the fluorescence anisotropy of the probe in a Spex spectrofluorometer (Fluorolog 1691) (excitation wavelength 492 nm, emission wavelength 570 nm, 16-nm slits; a cut-off filter of 550 nm was employed in the emission pathway to eliminate any contribution due to scattered light). The device was equipped with a stopped-flow module designed and built at the Laboratory of Biomolecular Dynamics (K. U. Leuven). Flutax-2 is photostable under these conditions, while Flutax-1 shows appreciable photoquenching (1% of the total intensity per second) during the measurement. The dead time of the instrument was measured as described above and was found to be ~10 ms. A minimum of 8 curves were averaged for each measurement. The slower dissociation of Flutax-1 and Flutax-2 from microtubules was measured by the decrease in fluorescence anisotropy in the SLM-8000D fluorometer equipped with a home-built mixing device consisting of two 1-ml syringes fixed to a thermostated aluminum block in such a way that they moved simultaneously and connected to a three-way Hamilton valve, which acted as a mixing chamber. The output of the valve was connected to the cuvette. The dead time of the complete system was about 2 s, comparable with the 1-s time constant employed in the fluorometer.

The fitting of the kinetic curves was done using a nonlinear least squares fitting program based on the Marquardt algorithm (36) when pseudo-first order conditions were used; otherwise, the FITSIM package (38) was employed.

X-ray Scattering by Microtubule Solutions—Measurements were made at station 2.1 of the Daresbury Laboratory Synchrotron Radiation Source. Instruments employed, data acquisition and processing, and interpretation of the microtubule x-ray scattering were as described previously (23).

RESULTS

In order to determine the signal to monitor the binding of the fluorescent taxoids, the spectroscopic properties of the bound and free Flutax-1 and Flutax-2 were investigated. Fig. 1 shows

[2] J. A. Evangelio and J. M. Andreu, unpublished observations.

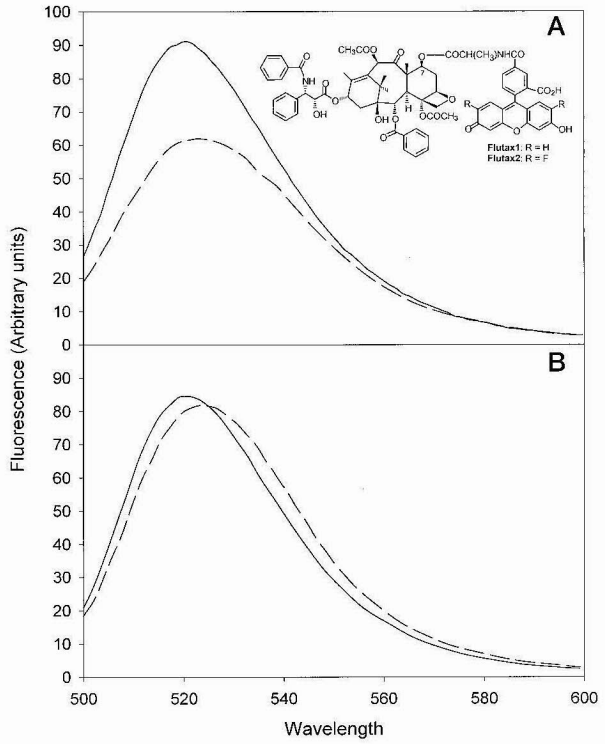

FIG. 1. *A*, fluorescence emission spectra of 1 μM Flutax-1 in GAB buffer in presence of microtubules assembled from 20 μM tubulin before λ_{max} = 521 nm (*solid line*) and after λ_{max} = 522 nm (*dashed line*) being displaced by 50 μM docetaxel. *B*, 1 μM Flutax-2 in GAB buffer in the presence of microtubules assembled from 20 μM tubulin before λ_{max} = 520 nm (*solid line*) and after λ_{max} = 524 nm (*dashed line*) being displaced by 50 μM docetaxel. The spectra were taken in a Shimadzu RF-540 spectrofluorometer, the excitation wavelength was 480 nm, and the bandwidth of the excitation and emission slits was 5 nm. The chemical structure of both probes is shown in *A*.

TABLE I
Anisotropy of the fluorescence emission of the fluorescent taxoids (1 μM) in GAB at 37 °C (λ_{ex} = 470 nm, λ_{cms} = 560 nm)

Ligand	Free	Bound[a]	Displaced[a]
Flutax1	0.05 ± 0.02	0.24 ± 0.02	0.05 ± 0.02
Flutax2	0.04 ± 0.01	0.26 ± 0.02	0.08 ± 0.01

[a] Bound to microtubules assembled from 20 μM pure tubulin in GAB or displaced by the addition of 50 μM docetaxel.

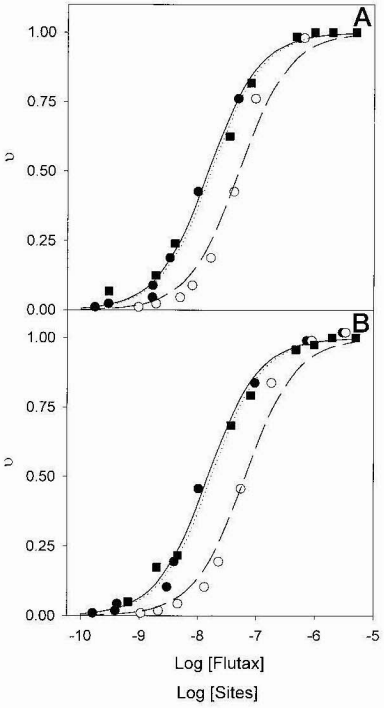

FIG. 2. *A*, *solid line* and *circles*, titration curve of 1 μM taxoid sites in stabilized microtubules with Flutax-1 at 27 °C measured by centrifugation; data are corrected for the percentage of inactive ligand. *Dashed line* and *open circles*, uncorrected data and fit. A small part of the ligand in use was found to be inactive, since it remained in the supernatant at very high concentrations of microtubules, disturbing the measurement of the free ligand concentration and artifactually decreasing the apparent binding constant measured. This effect was corrected as described under "Experimental Procedures." This percentage was found to be 4 ± 1% in the case of Flutax-1 and 6 ± 1% in the case of Flutax-2. *Solid squares* and *dotted line*, titration curve of 25 nM Flutax-1 with taxoid sites in stabilized microtubules measured by anisotropy. *B*, *solid line* and *circles*, titration curve of 1 μM taxoid sites in stabilized microtubules with Flutax-2 at 27 °C corrected for the percentage of inactive ligand. *Dashed line* and *open circles*, uncorrected data. *Solid squares* and *dotted line*, titration curve of 25 nM Flutax-2 with stabilized microtubules measured by anisotropy.

the fluorescence emission spectra of the bound and free forms of Flutax-1 and Flutax-2. To match the scattering contribution of microtubules, the spectrum of the free species was obtained by displacing the bound form with a large excess of the nonfluorescent taxoid docetaxel. This closely related compound binds to the Taxol binding site and has a larger solubility (10). Centrifugation of the solution after displacement confirmed that the fluorescent taxoids were dissociated from the microtubules. It can be seen clearly that the fluorescence intensity of the bound form of Flutax-1 is 50% larger than that of the free form. The spectrum shows a small shift toward the blue. The emission spectrum of bound Flutax-2 shows a larger shift toward the blue but a smaller change in fluorescence intensity. The intensity change is due to the shift of the ionization equilibrium of the fluorescein group upon binding (24); *i.e.* the bound group is mostly in the dianionic form, which has a larger quantum yield than the monoanion. By choosing adequately the pH of the buffer, it was possible to maximize the change of intensity of fluorescence upon binding, which was found to be optimum at pH 6.5. Since the p*K* value for the ionization of the difluorofluorescein group of Flutax-2 is much lower than that of Flutax-1, little change in fluorescence is observed upon binding to its site.

In addition, the immobilization of the fluorescent group that results from the binding reaction produces a large increase in the fluorescence anisotropy of Flutax-1 and Flutax-2. The anisotropy values of these probes under different conditions are shown in Table I.

Equilibrium Binding of Fluorescent Taxoids to Cross-linked Microtubules—The equilibrium constants of binding of Flutax-1 and Flutax-2 to microtubules assembled from pure tubulin in GAB were measured by sedimentation and anisotropy using diluted cross-linked microtubules. This was necessary, since in preliminary experiments using nonstabilized microtubules, the reaction was essentially displaced toward the bound ligand state due to the high concentration of binding sites. The cross-linking employed did not affect the binding stoichiometry or the kinetics of binding (described below).

The titration curves (corrected for the small percentage of inactive ligand in the experiments in the case of the sedimentation assays) are shown in Fig. 2. The stoichiometry was found to be 1:1 (0.99 ± 0.07 mol of Flutax-2/mol of assembled tubulin), and the affinity was high (K_a = 6.6 ± 1.0 × 10^7 M^{-1} (centrifugation) or 6.0 ± 0.2 × 10^7 M^{-1} (anisotropy) for Flutax-1, and K_a = 6.1 ± 1.7 × 10^7 M^{-1} (centrifugation) or 5.9 ± 0.3 × 10^7 M^{-1} (anisotropy) for Flutax-2 at 27 °C). The affinity constants determined at different temperatures are

TABLE II
Equilibrium constants of fluorescent taxoids binding to microtubules.

Ligand	As determined by equilibrium measurements ($K_a \times 10^7$ M^{-1})					
	22 °C	27 °C	32 °C	37 °C	40 °C	42 °C
Flutax-1[a]	12.2 ± 2.1	6.6 ± 1.0	4.6 ± 1.5	2.6 ± 0.7	1.5 ± 0.3	ND[b]
Flutax-1[c]	ND	6.0 ± 0.2	4.3 ± 0.4	2.9 ± 0.3	2.1 ± 0.2	1.5 ± 0.1
Flutax-2[a]	10.8 ± 3.5	6.1 ± 1.7	4.0 ± 0.4	2.0 ± 0.7	1.0 ± 0.2	ND
Flutax-2[c]	ND	5.9 ± 0.3	4.2 ± 0.2	2.2 ± 0.2	2.0 ± 0.1	1.8 ± 0.2

	As calculated from the kinetic measurements				
	Flutax-2				Flutax-1 (37 °C)
	32 °C	35 °C	37 °C	39 °C	
K_1 ($\times 10^5$ M^{-1})	13.9 ± 8.1	8.1 ± 6.1	8.4 ± 1.2	6.8 ± 4.1	6.2 ± 2.6
K_2	134 ± 44	109 ± 50	123 ± 45	98 ± 44	12 ± 5
K_{OVR} ($\times 10^7$ M^{-1})	18.8 ± 8.2	8.9 ± 6.1	10.4 ± 5.5	6.8 ± 4.4	0.8 ± 0.6

[a] Data from centrifugation measurements.
[b] ND, not determined.
[c] Data from anisotropy measurements.

summarized in Table II. The reactions were exothermic and characterized by negative entropy changes (Table IV).

Kinetics of Binding of Flutax-1 and Flutax-2 to Microtubules Followed by Fluorescence Intensity—The mechanism of Taxol binding to microtubules was studied with kinetic methods. The binding reaction was found to be very fast, requiring stopped-flow techniques. The length of the microtubules before and after passing through the stopped flow system was checked using electron microscopy (average length 4.85 ± 2.15 nm and 3.70 ± 2.10 nm, respectively), and their morphology was found to be normal.

Fig. 3*A* (*curve a*) shows the time course of binding of Flutax-1 to a 20-fold excess of microtubule sites. Microtubules have been assembled from pure tubulin in GAB at 37 °C. To check that the change of fluorescence is due to the specific binding of the probe to the Taxol site on the microtubules, the same experiment was performed with microtubules saturated with a non-fluorescent taxoid (docetaxel); in this case, no change of fluorescence can be observed (Fig. 3*A*, *curve b*). The kinetics of the reaction can be expressed as one single exponential; a fitting to a sum of two or more exponentials does not improve the residuals and yields practically identical rate constants, indicating that a single process is observed. Fig. 3*B* shows the dependence of the observed rate constant on the concentration of sites at different temperatures. The observed rate constant depends linearly on the concentration of sites (calculated for each experiment from the critical tubulin concentration, measured as described in Ref. 10), indicating a simple mechanism for the binding of the ligand to its site.

$$\text{Flutax} + \text{site} \underset{k_{-1}}{\overset{k_{+1}}{\rightleftharpoons}} \text{Flutax·site}$$

SCHEME 1

With such a model, the observed rate constant under pseudo-first order conditions depends on the rate constants k_{+1} and k_{-1} as follows.

$$k_{obs} = k_{+1}[\text{sites}] + k_{-1} \quad \text{(Eq. 1)}$$

From the representation in Fig. 3*B*, it is possible to determine k_{+1} from the slope of the regression and k_{-1} from the extrapolation of the regression to concentration zero. The value of k_{+1} can be obtained with sufficient precision. But in order to obtain the value of the dissociation constant with enough precision, the value of the product k_{+1}*[sites] has to be low enough so that k_{-1} has a significant weight in k_{obs}. In order to do that, the concentration of tubulin has to be 1 order of magnitude lower than the one necessary to assemble microtubules. These concentrations were achieved employing cross-linked microtubules; in this way, the concentration of sites can be decreased, and the value of k_{-1} can be properly determined. The results of these experiments are shown in an *inset* of Fig. 3*B*. The values of k_{+1} obtained with cross-linked microtubules were very similar to those obtained with normal microtubules (Table III).

Measuring the rate constants of the binding of Flutax-2 to

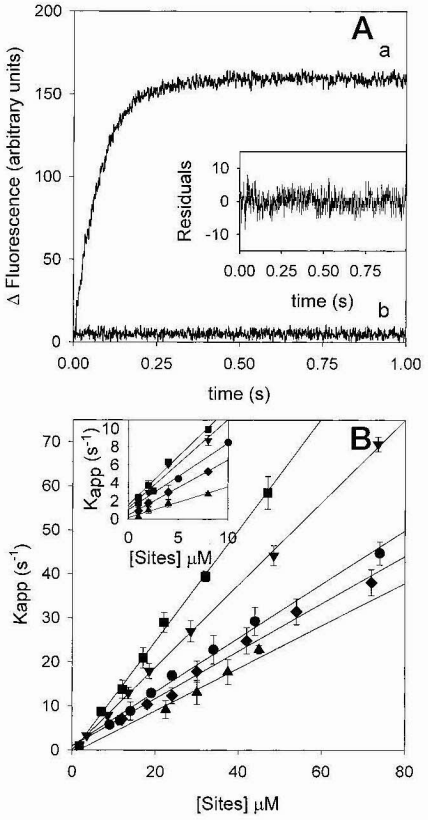

FIG. 3. *A*, kinetics of binding of Flutax-1 to microtubules at 35 °C. In the stopped-flow device, a 1 μM solution of Flutax-1 was mixed with 25 μM pure tubulin assembled into microtubules (concentration of sites, 20 μM) (final concentrations of 500 nM Flutax and 10 μM sites) in the absence (*a*) and presence (*b*) of 50 μM docetaxel. *Curve a* is fitted to an exponential decay. *Inset*, residues between the experimental and theoretical curves. *B*, dependence on the concentration of sites of the observed rate constants of binding of Flutax-1 (500 nM) at 32 °C (*triangles*), 35 °C (*diamonds*), 37 °C (*circles*), 39 °C (*inverted triangles*), and 42 °C (*squares*) to microtubules assembled from pure tubulin in GAB. The *solid lines* are the best fittings to the experimental data. *Inset*, dependence on the sites concentration for the binding of Flutax-1 (50 nM) to cross-linked microtubules.

TABLE III
Kinetic constants of binding (k_{+1}, k_{+2}) and dissociation (k_{-1}, k_{-2}) of fluorescent taxoids from microtubules

	32 °C	35 °C	37 °C	39 °C	42 °C
Flutax-1					
k_{+1} ($\times 10^5$ M^{-1} s^{-1})[a]	3.65 ± 0.29	5.38 ± 0.26	6.10 ± 0.22	9.36 ± 0.11	12.65 ± 0.25
k_{+1} ($\times 10^5$ M^{-1}s^{-1})[b]	3.43 ± 0.15	6.12 ± 0.22	7.43 ± 0.26	9.83 ± 0.14	11.74 ± 0.10
k_{-1} (s^{-1})[b]	0.16 ± 0.04	0.45 ± 0.18	0.99 ± 0.27	1.21 ± 0.42	1.55 ± 0.33
k_{+2} (s^{-1})[a,c]	ND[d]	ND	0.3 ± 0.1	ND	ND
Flutax-2					
k_{+1} ($\times 10^5$ M^{-1} s^{-1})[b]	4.15 ± 0.70	5.66 ± 0.50	13.83 ± 0.18	12.35 ± 0.90	17.72 ± 0.72
k_{-1} (s^{-1})[b]	0.30 ± 0.18	0.70 ± 0.41	1.63 ± 0.18	1.81 ± 0.67	2.38 ± 0.49
k_{+2} (s^{-1})[a,c]	1.9 ± 0.5	2.1 ± 0.8	2.7 ± 0.8	2.6 ± 1.0	ND

	20 °C	25 °C	30 °C	35 °C	37 °C	40 °C	42 °C
Flutax-1							
k_{+2} ($\times 10^{-2}$ s^{-1})[a,e]	0.29 ± 0.03	0.59 ± 0.01	1.05 ± 0.05	1.79 ± 0.07	2.43 ± 0.07	3.61 ± 0.20	4.53 ± 0.10
k_{-2} ($\times 10^{-2}$ s^{-1})[a,c]	ND	0.50 ± 0.05	1.16 ± 0.07	2.13 ± 0.13	2.61 ± 0.12	ND	ND
Flutax-2							
k_{-2} ($\times 10^{-2}$ s^{-1})[a,c]	0.43 ± 0.03	0.71 ± 0.04	1.36 ± 0.03	1.92 ± 0.10	2.20 ± 0.12	2.71 ± 0.13	3.43 ± 0.21

[a] Data obtained with non-cross-linked microtubules.
[b] Data obtained with cross-linked microtubules.
[c] Data obtained by measuring the change in fluorescence anisotropy.
[d] ND, not determined.
[e] Data obtained by measuring the change in fluorescence intensity.

microtubules is more difficult, since very little change in fluorescence intensity is observed upon binding to its site. Nevertheless, it is possible to follow the reaction due to the shift to the blue of the spectrum (Fig. 1*B*). By using a 530-nm cut-off filter (coincident with the isosbestic point), the part of the spectrum at which the intensity of the bound form is smaller than that of the free form can be selected. It is possible then to monitor the binding reaction by the small decrease of the observed fluorescence intensity (Fig. 4*A*). In this way, the values of k_{+1} and k_{-1} for the binding of Flutax-2 to the taxoid binding site can be determined. As in the case of Flutax-1, the binding reaction is monophasic (within the experimental indetermination due to the much lower signal/noise ratio) and is blocked by docetaxel. The observed kinetic rate depends linearly on the concentration of sites (Fig. 4*B*). The kinetic constants of the binding of Flutax-1 and Flutax-2 to its site are summarized in Table III.

Kinetic Homogeneity of the Binding Sites—Since the change in fluorescence occurs in the ligand and not in the protein, the reactant in excess to achieve pseudo-first order conditions needs to be the assembled tubulin. The use of microtubules as the ligand in excess implies the assumption that all of the sites in the microtubule are equal. Since the site of Taxol in microtubules has been mapped in the lumen of the tube using electron diffraction, electron microscopy, and docking methods (30, 34), it might be possible that the drug has to diffuse through the ends of the tube or through openings in the tube wall in order to gain access to the site. In this way, the sites closer to the outer solution would be more accessible than the more internal sites. When those sites are in excess over the drug (under the pseudo-first order conditions), it might be possible that only the outer ones become filled. To evaluate this possibility, experiments were performed at equimolecular concentrations (5, 10, and 20 μM) of Flutax-1 and sites, and the resulting kinetic curves were analyzed using the proposed kinetic model (Scheme 1) with the kinetic analysis package FITSIM (38) (Fig. 5). The data fit the predicted bimolecular reaction scheme with the same kinetic constants within the experimental error as those determined under pseudo-first order conditions, thus demonstrating that all taxoid binding sites in the microtubule are equal from the kinetic point of view.

On the other hand, structural differences, like changes in the number of protofilaments or microtubule openings, might affect the kinetics of binding. Microtubule solutions assembled from purified tubulin consist of a mixture of microtubules with a different number of protofilaments typically ranging from 11 to 15 (26) and have a certain percentage of open microtubules. If microtubule-organizing centers are used to nucleate microtubule growth, the number of protofilaments in microtubules assembled from pure tubulin is fixed at 13, and the fraction of open microtubules is reduced (39, 40). Microtubules were assembled from pure tubulin in GAB in the presence of 1, 2, and 5% (w/w) axonemes from sea urchin sperm (it was checked by electron microscopy that most of the microtubules were attached to the axonemes). The observed kinetics of Flutax-1 binding were not affected by the presence or absence of axonemes (k_{+1} at 37 °C was 6.27 ± 0.51 M^{-1} s^{-1}; with 1% axonemes, 6.38 ± 0.43 M^{-1} s^{-1}; with 2% axonemes, 6.36 ± 0.38 M^{-1} s^{-1}; with 5% axonemes, 6.39 ± 0.49 M^{-1} s^{-1}). This indicates that the kinetics of binding of the fluorescent taxoid were not significantly modified by the heterogeneity of *in vitro* assembled microtubules.

Kinetics of Binding of Flutax-1 and Flutax-2 to Microtubules Followed by Fluorescence Anisotropy—A large change in the fluorescence anisotropy of the probe is observed upon binding (Table I). The process was studied with stopped-flow anisotropy measurements in order to obtain more information about the binding reaction. Fig. 6*A* shows the time course of the binding of Flutax-1 to microtubules followed both by the change in intensity (*inset*) and anisotropy of the fluorescence. It can be seen that the change in fluorescence anisotropy is much slower than the change in intensity. The apparent rate constant of the anisotropy change upon binding is very weakly dependent on the concentration of sites (k_{obs} with 5 μM sites, 0.22 ± 0.07 s^{-1}; 10 μM sites, 0.26 ± 0.04 s^{-1}; 20 μM sites, 0.28 ± 0.05 s^{-1}; 37 °C), indicating that a monomolecular reaction is observed. The change in anisotropy can be expressed with a single exponential, indicating that a single process is being observed (within the experimental limitations due to the technical difficulty of the measurement; see "Experimental Procedures"). The change in anisotropy is blocked by docetaxel. Since photostability controls showed that Flutax-1 suffers photolysis (about 17% of the total intensity during the experiment), measurements were done mainly with Flutax-2, which is devoid of this effect. Fig. 6*B* shows the time course of Flutax-2 binding to microtubules. The observed rate constant is much slower than that measured by the fluorescence intensity change and shows a weak dependence on the concentration of binding sites (k_{obs} 5

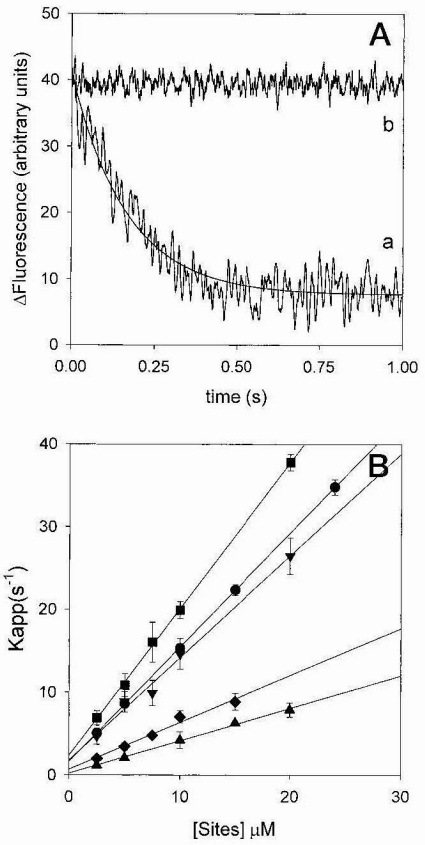

FIG. 4. *A*, kinetics of binding of Flutax 2 to microtubules at 35 °C. A 500 nM solution of Flutax-2 was mixed with 20 μM sites in cross-linked microtubules of pure tubulin in GAB in the stopped-flow device (final concentrations of 250 nM Flutax-2 and 10 μM sites) in the absence (*a*) and presence (*b*) of 50 μM docetaxel. The *solid line* is the best fit. Data were averaged in 5-ms intervals. *B*, dependence on the concentration of sites in the cross-linked microtubules of the observed rate constants of binding of Flutax-2 (250 nM) at 32 °C (*triangles*), 35 °C (*diamonds*), 37 °C (*circles*), 39 °C (*inverted triangles*), and 42 °C (*squares*) to microtubules assembled from pure tubulin in GAB. The *solid lines* are the best fittings to the experimental data.

μM sites, 1.40 ± 0.61 s^{-1}; 10 μM sites, 1.66 ± 0.54 s^{-1}; 20 μM sites, 2.21 ± 0.78 s^{-1}; 37 °C).

The data suggest that the change in anisotropy is due to a second monomolecular reaction subsequent to the high affinity binding of the taxoid to its site. Such a rearrangement cannot be observed by fluorescence intensity unless there is a displacement of the equilibrium of the first step or a change in the intensity due to this second step. The reaction should then follow the following mechanism.

$$\text{Flutax} + \text{site} \underset{k_{-1}}{\overset{k_{+1}}{\rightleftharpoons}} \text{Flutax·site} \underset{k_{-2}}{\overset{k_{+2}}{\rightleftharpoons}} \textit{Flutax} \cdot \textit{site}^*$$

SCHEME 2

Where the first equilibrium entails the intensity change and the second one the anisotropy change, the kinetic rate constant observed with the change in anisotropy is as follows.

$$k_{S(\text{obs})} = \frac{K_1 k_{+2}[\text{sites}]}{1 + K_1[\text{sites}]} + k_{-2} \qquad \text{(Eq. 2)}$$

The weak dependence of the observed rate constant on the concentration of sites (together with the large measurement error) precludes the precise determination of the k_{-2} and K_1 constants, but k_{+2} can be measured and the order of magnitude of K_1 can be determined with a moderate accuracy if the value

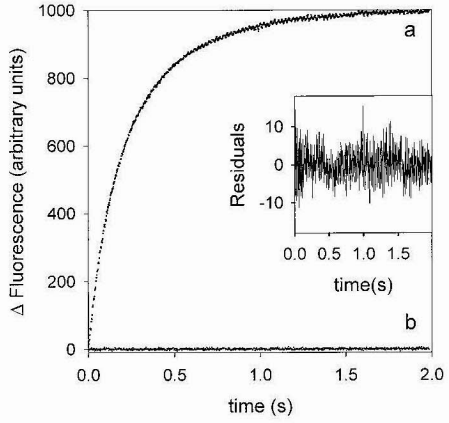

FIG. 5. **Kinetics of binding of 5 μM Flutax-1 to 5 μM sites in microtubules assembled from pure tubulin in GAB in the absence (*a*) and presence (*b*) of 100 μM docetaxel.** The data were fitted using the reaction model I; the obtained kinetic constants were $k_{+1} = 6.30 \pm 0.10 \times 10^5\ M^{-1}\ s^{-1}$ and $k_{-1} = 1.17 \pm 0.38 \times 10^{-2}\ s^{-1}$ (see Table III for comparison). *Inset*, residues between the experimental and theoretical curves.

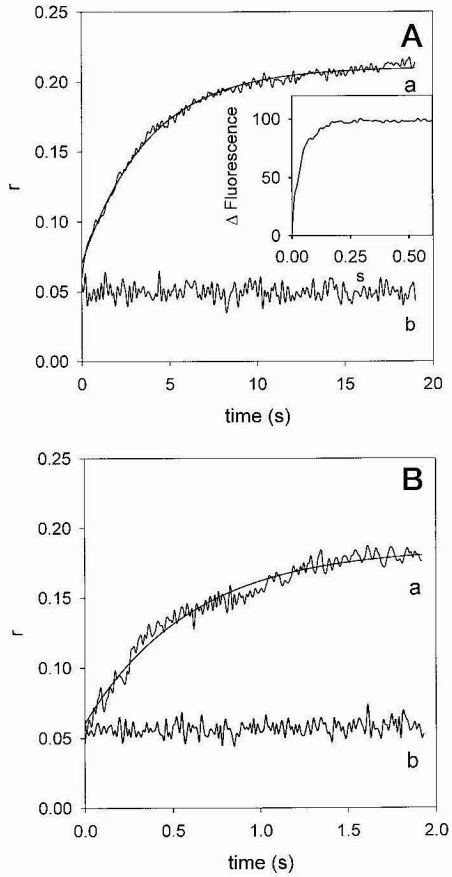

FIG. 6. *A*, kinetics of binding of Flutax-1 to microtubules at 37 °C. In the anisotropy stopped-flow device, a 1 μM solution of Flutax-1 was mixed with 24 μM pure tubulin assembled into microtubules (concentration of sites 20 μM) (final concentrations of 500 nM Flutax and 10 μM) in the absence (*a*) and presence (*b*) of 50 μM docetaxel. *Inset*, kinetics of binding of Flutax of the same sample followed by the change in fluorescence intensity. *B*, kinetics of binding of Flutax-2 to microtubules at 37 °C. In the anisotropy stopped-flow device, a 1 μM solution of Flutax-2 was mixed with 24 μM pure tubulin assembled into microtubules (concentration of sites 20 μM) (final concentrations of 500 nM Flutax and 10 μM sites) in the absence (*a*) and presence (*b*) of 50 μM docetaxel. *Curve a* is fitted to an exponential decay.

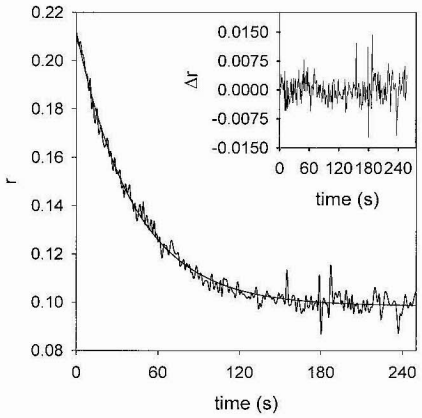

FIG. 7. **Kinetics of dissociation of Flutax-2 from microtubules at 35 °C.** At time 0 s, 200 μM docetaxel was mixed 1:1 with to 20 μM tubulin in GAB assembled into microtubules that contained 15 μM Flutax-2 bound (final concentrations: 100 μM docetaxel, 10 μM tubulin, 7.5 μM Flutax-2). The reaction was followed by the change in anisotropy. The data are fitted to a single exponential. *Inset*, residues between the experimental and theoretical curves.

of k_{-2} obtained from the dissociation measurements (see below) is used. K_1 can be estimated to be on the order of 10^6 M^{-1} (similar to the ones measured from the change in intensity) in the range of temperatures studied. The kinetic data obtained by measuring the change of anisotropy upon binding of Flutax-1 and Flutax-2 to its site are summarized in Table III.

Kinetics of Dissociation of Flutax-1 and Flutax-2 from Microtubules—The dissociation rate constant can be measured by displacing the fluorescent drug bound to microtubules with a large excess of a nonfluorescent competitor. Assuming the product k_{+1}*[docetaxel] is much higher than k_{-1}, all of the free sites are rapidly filled with docetaxel, and the reaction (Scheme 2) is displaced toward the left side at a kinetic rate of k_{-1} or k_{-2}, depending on the limiting step. Since the condition is fulfilled and the concentration of docetaxel is 100 μM, k_{+1} for docetaxel has to be in within 1 order of magnitude with k_{+1} of Flutax-1 and Flutax-2. The dissociation reaction followed by fluorescence intensity and anisotropy for Flutax-1 had identical rate constants. An example of dissociation of Flutax-2 is shown in Fig. 7. The values of the rate constants of dissociation (Table III) were much lower than the values determined for k_{-1}, indicating that the rate-limiting step of the reaction is the reversal of the conformational transition (k_{-2}). Control measurements with cross-linked microtubules indicated that the dissociation rate constant is not affected by cross-linking (k_{-2} = 2.51 ± 0.14 × 10^{-2} s^{-1}, Flutax-1, 37 °C).

Thermodynamic Parameters of Binding of Fluorescent Taxoids—Analyzing the dependence on the temperature of the kinetic constants of the individual steps of the reaction and the equilibrium constants of binding, it is possible to obtain the thermodynamic parameters of the overall and individual reactions of binding (Table IV). The kinetics of the reaction were fully characterized for Flutax-2 only due to the limited photostability of Flutax-1. The Arrhenius plots of the individual binding and dissociation reactions of Flutax-2 are shown in Fig. 8*A*, and the reaction scheme is shown in Fig. 8*B*. The enthalpy and entropy values obtained from the kinetic measurements and from the equilibrium measurements are compatible (Table IV). The binding of Flutax-1 and Flutax-2 to their site in microtubules assembled from purified tubulin is exothermic and enthalpy-driven, the overall entropy change being negative.

Microtubule Structural Changes Induced by Flutax-1 and Flutax-2 Binding to Microtubules—Small angle x-ray solution scattering and electron microscopy results have shown that the addition of Taxol to preformed microtubules produces a 0.8-nm reduction of the mean diameter and in the mean number of protofilaments of the microtubules from 13.1 to 12.3 (23). Similar experiments have been performed, adding Flutax-1 and Flutax-2 to preassembled microtubules in GAB buffer. Unexpectedly, a displacement in the positions of the J_0 maxima of the x-ray scattering profile toward a smaller value has been measured (Table V, Fig. 9*A*), indicating a 9% increase in the mean diameter of the microtubules. Therefore, Flutax-1 and Flutax-2 microtubules should have an average of 14.3 protofilaments, roughly one protofilament more than control microtubules, contrary to the result with Taxol.

The time course of the change in position of the J_{01} maxima induced by Flutax-2 on glycerol microtubules was measured (Fig. 9*B*). The results showed a time-dependent displacement between the expected values, distinct from the noise of the individual kinetic measurement, with a half-life of approximately 60 s under the conditions of these experiments, similar to the change induced by Taxol (23). Nevertheless, it should be pointed out that this structural rearrangement should affect neither the binding equilibrium measurements, since it should be blocked by cross-linking the microtubules, nor the kinetic measurements, since it cannot be observed in the time ranges employed in the kinetic measurements.

DISCUSSION

Mechanism of Binding of Fluorescent Taxoids to Microtubules—Two fluorescent derivatives of Taxol, Flutax-1 and Flutax-2, are used in this work as probes for the Taxol binding site. The interaction of Flutax-1 and Flutax-2 with microtubules is a fast bimolecular reaction followed by at least two monomolecular rearrangements of the system. The first step is a fast binding of the ligand with micromolar affinity. This reaction does not affect the mobility of the fluorescent group (either fluorescein or difluorofluorescein), and since it is blocked by docetaxel it seems to be contributed by the binding of the Taxol moiety itself. Subsequent to the bimolecular step, there is a monomolecular reaction, which involves a rearrangement in the system, resulting in the immobilization of the fluorescent group. This step probably implies a weak binding of the fluorescein moiety to the microtubules. The tight binding of these Taxol derivatives has been recently characterized by measurements of fluorescence lifetimes and polarization of the bound forms with picosecond time resolution, showing that the interaction with the protein shifts the fluorescein chromophore toward the dianion structure.[3] The last step observed is a slower relaxation of the microtubule structure, which implies an increase in the mean radius of the microtubules from 12.1 to 13.2 nm, opposite of that observed with Taxol (23). This supports the notion of microtubule wall dynamics (23) and the existence of a certain interaction of the fluorescent moieties of the probes with microtubules, which modifies the lateral interactions between protofilaments.

There are strong reasons to assume that Flutax-1 and Flutax-2 are *bona fide* probes of the Taxol binding site, taking into account the differences in size and charge due to the fluorescent moiety and its effects. These include the following. 1) Flutax-1, Flutax-2, Taxol, and docetaxel are able to induce the assembly of inactive GDP-tubulin (10, 24). 2) All of them compete for the same site with affinities in the same range of magnitude (10, 23, 24). 3) Docetaxel blocks the Flutax binding reaction at its first step (this is a direct consequence of binding the same site). 4) The Flutax dissociation results imply that the kinetic rate of binding of docetaxel should be in the same order of magnitude as those of Flutax-1 and Flutax-2. 5) Polymor-

[3] O. Cañadas, P. Lillo, and A. U. Acuña, manuscript in preparation.

TABLE IV
Thermodynamic parameters of binding of Flutax and Flutax-2 to microtubules

	Flutax-1	Flutax-2
Parameters determined from the binding equilibrium measurements		
ΔH_{app} kJ mol^{-1}	-84 ± 7^a $(-70 \pm 8)^b$	-95 ± 10^a $(-67 \pm 11)^b$
ΔS_{app} J mol^{-1} K^{-1}	-132 ± 23^a $(-85 \pm 21)^b$	-174 ± 33^a $(-76 \pm 25)^b$
Parameters determined from the kinetic measurements		
Ea_1 kJ mol^{-1}	101 ± 8	122 ± 27
Ea_{-1} kJ mol^{-1}	184 ± 35	174 ± 22
ΔH_1 kJ mol^{-1}	-84 ± 36	-52 ± 25
ΔS_1 J mol^{-1} K^{-1}	-150 ± 126	-38 ± 60
Ea_2 kJ mol^{-1}	ND[c]	41 ± 12
Ea_{-2} kJ mol^{-1}	94 ± 3	71 ± 3
H_2 kJ mol^{-1}	ND	-30 ± 12
S_2 J mol^{-1} K^{-1}	ND	-53 ± 40
ΔH_{OVR} kJ mol^{-1}	ND	-82 ± 20
ΔS_{OVR} J mol^{-1} K^{-1}	ND	-91 ± 51

[a] Data from centrifugation measurements.
[b] Data from anisotropy measurements.
[c] ND, not determined.

phism in microtubule protofilament number does not affect the binding and dissociation kinetics; mixtures of microtubules with different protofilament number behave homogeneously from the kinetic point view.

The first two steps of the reaction of Flutax-2 binding are similar from the thermodynamic point of view; both the binding of the Taxol group to its site and the conformational change are exothermic and entropically disfavored, so the reaction is enthalpy-driven (Fig. 8*B*). The first step of the reaction, the binding itself, has large activation energy, even with a fast kinetic constant (*i.e.* a large preexponential factor), indicating that the entrance and exit of the ligand from its site are relatively difficult. The second step has a lower activation energy; however, it is a slow reaction. In both steps of the reaction, the change in entropy is negative, as expected from a reaction that implies the loss of degrees of freedom.

The equilibrium constants calculated from the kinetic data for Flutax-2 are about 5 times larger than the equilibrium measured ones, while those calculated for Flutax-1 are 3 times smaller (Table II). These differences give offsets of -4 kJ mol^{-1} and 3 kJ mol^{-1} in the global free energy changes of binding of Flutax-2 and Flutax-1, respectively, whereas the enthalpy and entropy change values are compatible. They cannot be attributed to the structural change of the microtubules (see "Results"). Since any possible fast equilibrium between an active and an inactive conformer of Flutax-2 in the solution would decrease both the binding constant and the kinetic rate of the bimolecular binding reaction, we cannot offer at present an explanation of these small differences between the kinetic and equilibrium measurements. The taxoid binding affinities (Table II) were high (on the order of 10^7 M^{-1}). Apparent binding constants (from measurements necessarily affected by the linkage of binding and microtubule elongation (see Introduction)) previously reported for other taxoids were as follows: 2-debenzoyl-2-(*m*-aminobenzoyl)Taxol, $2.0 \pm 0.9 \times 10^7$ M^{-1} (21); 3′-*N*-*m*-aminobenzamido-3′-*N*-debenzamido-Taxol, $1.63 \pm 0.16 \times 10^7$ M^{-1} (high affinity site) (25); and Taxol, 1.15×10^7 M^{-1} (12).

The free energy change of binding of Flutax-2 to its site at 37 °C is 48 ± 2 kJ mol^{-1}, roughly 35 kJ mol^{-1} of them coming from the initial step including the binding of the Taxol moiety and 13 kJ mol^{-1} coming from the immobilization of the fluorescein group, which contributes significantly to the binding constant (note that the binding of isolated fluorescein would not be observed, since the intrinsic affinity is far too low, K_2 of ~10 for Flutax-1 and 100 for Flutax-2). These values imply that if the presence of the fluorescent group did not in any way disturb the binding of the taxoid group, the affinity of Flutax-2 should be larger than that of Taxol. Nevertheless, competition studies of the binding of Flutax-2 and Taxol with Rotax (7-*O*-[*N*-4-tetramethylrhodaminecarbonyl)-L-alanyl]Taxol) for its site indicate that Taxol has an affinity similar to that of Flutax-2.[2]

Stabilized Taxoid Binding Sites Provided by Cross-linked Microtubules—In order to be able to precisely measure binding and kinetic constants of ligands with high affinities or fast binding reactions, low concentrations of binding sites are required. Unfortunately, due to the mechanism of microtubule assembly, a condensation nucleation polymerization (41), in which a free tubulin concentration over a certain limit (so called critical concentration) is necessary to keep the protein assembled, purified microtubules are naturally unstable against dilution (42–43). The system has an additional complication; tubulin undergoes relatively fast aging even at 4 °C (44). This means that purified tubulin manipulation to produce microtubules is a relatively complex procedure. A treatment widely used to prevent microtubule disassembly by dilution and low temperature is a mild fixation with glutaraldehyde (45–47). 0.2% glutaraldehyde has been used to fix the cytoskeleton of Ptk2 cells, maintaining their ability to specifically bind Flutax-1 (24). In this work, we have demonstrated that this treatment conserves the taxoid binding properties of the microtubules *in vitro*. The binding stoichiometry and the kinetic parameters of the binding are unaffected by the fixation treatment. The bound Flutax-1 or Flutax-2 is displaced from the site by the nonfluorescent docetaxel, indicating that the binding is specific. These results show that cross-linked microtubules can be a very useful tool in the study of the taxoid-microtubule interactions.

The search of drugs whose targets are microtubules is a fundamental task in anticancer research. Since fixed microtubules are not dependent on temperature or GTP supply, they can be stored at low temperatures ready for use (for a week at 4 °C and probably for larger periods at lower temperatures; nevertheless, they cannot be frozen in the buffer employed).

Ligand Access to the Taxol Binding Site—In a previous study (23), it was shown that the Taxol binding sites in microtubules were easily accessible; bound Taxol exchanges with docetaxel and modifies the structure of previously assembled microtubules in 1 min. In that paper, we proposed several hypotheses on the possible mechanisms that may hold for Taxol to reach its site in the microtubules in the time range observed. The types of mechanisms proposed were as follows. 1) Taxol binds near

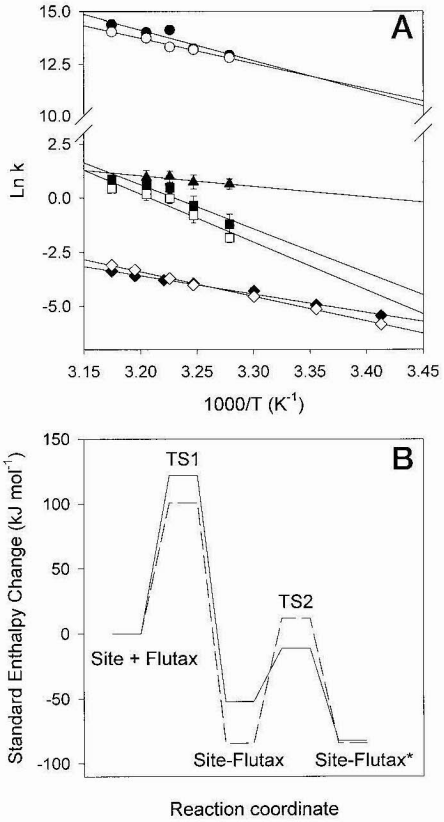

FIG. 8. *A*, Arrhenius plots of the observed kinetic reactions of the binding of Flutax-1 and Flutax-2 to their site in the microtubules assembled in GAB. *Open circles*, rate constant of association (k_{+1}) of Flutax-1 to its site in the microtubules. *Solid circles*, rate constant of association (k_{+1}) of Flutax-2 to its site in the microtubules. *Open squares*, rate constant of dissociation of Flutax-1 (k_{-1}) from its site in the microtubules. *Solid squares*, rate constant of dissociation of Flutax-2 (k_{-1}) from its site in the microtubules. *Solid triangles*, rate constant of the change toward the end state k_{+2} for Flutax-2. *Open diamonds*, rate constant of the change toward the intermediate state k_{-2} for Flutax-1 (*closed diamonds*) rate constant of the change toward the intermediate state k_{-2} Flutax-2. *B*, standard enthalpy change along the reaction pathway of binding of Flutax-1 (*dashed line*) and Flutax-2 (*solid line*) to microtubules. The reference state is the nonassociated mixture of Flutax and assembled tubulin. Note that the activation energy of the second step of the reaction and the total enthalpy charge of binding of Flutax-1 to microtubules are approximations calculated from the equilibrium measurements.

the outer microtubule surface. 2) Taxol binds into the lumen due to microtubule dynamic instability, permitting endwise depolymerization and reassembly with taxoid. 3) Taxol diffuses through the open microtubule ends and binds into the lumen. 4) Taxol diffuses through the microtubule wall and binds into the lumen. With the data available, mechanisms 2 and 3 could be definitively excluded, so only mechanisms 1 and 4 were left. Now, with the insight provided by the fast kinetic data now available, a more in depth discussion on ligand access to the binding site in the microtubules can be made.

The diffusion control limit for the binding of Flutax to microtubules can be estimated from the number of collisions of Flutax to a rod of the size of a microtubule (48) and can be calculated as follows,

$$k_{coll} = \frac{2 \times \pi \times Na \times (D_{Flutax} + D_{microtubules}) \times d_s}{\ln(L/r)} \qquad \text{(Eq. 3)}$$

where D values represent the diffusion constants of Flutax and microtubules (the diffusion coefficient for a molecule of the size of Flutax ($\sim 2 \times 10^{-9}$ m diameter) in an aqueous buffer containing 30% glycerol at 37 °C calculated using the Stokes-Einstein equation is 1.6×10^{-10} m^2 s^{-1}, while the value for the microtubule can be neglected); d_s is the reciprocal linear density of sites in the microtubule (6.15×10^{-10} m/site), L is the length of the microtubule, and r is its radius (12×10^{-9} m). Considering a 4×10^{-6}-m-long microtubule, the diffusion limit of the bimolecular rate will be 6.4×10^4 mol^{-1} m^3 s^{-1} (6.4×10^7 M^{-1} s^{-1}) (note that this number is a maximal estimation, since it does not consider the repulsive electrostatic interaction between the negative net charges of both molecules). The measured bimolecular rate constant of Flutax-2 binding to microtu-

TABLE V

Ligand-induced changes in the position of the x-ray solution scattering maxima of microtubules previously assembled from GTP-tubulin in glycerol buffer (see Fig. 9)

Ligand added	J_{01}	J_{02}	Mean helical radius
			nm
None	0.050	0.093	12.1
Taxol	0.053	0.099	11.3
Flutax-1	0.046	0.088	13.2
Flutax-2	0.046	0.088	13.2

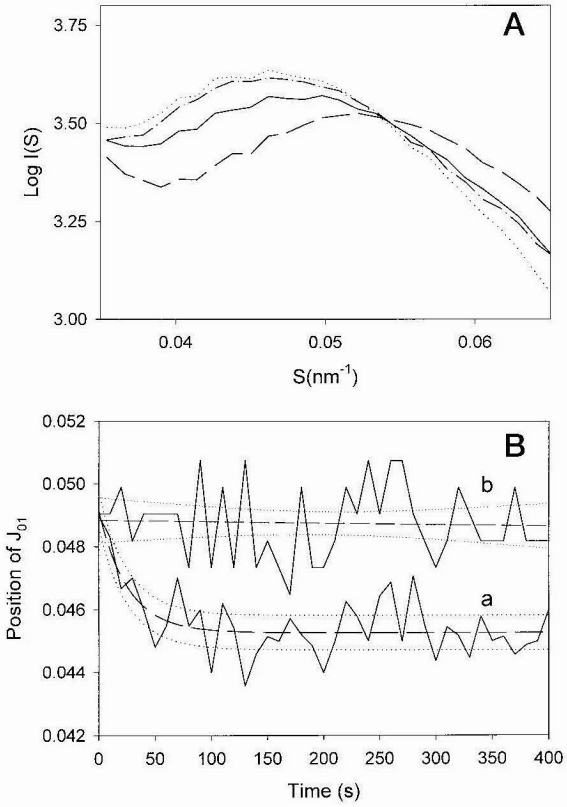

FIG. 9. **Taxoid-induced changes in microtubule x-ray scattering.** *A*, the intensity profiles of microtubules assembled from 67 μM GTP-tubulin in glycerol assembly buffer at 37 °C are shown. One hour after assembly, 1% Me_2SO (*solid line*), 70 μM Taxol plus 1% Me_2SO (*dashed line*), 70 μM Flutax-1 plus 1% Me_2SO (*dotted line*), or 70 μM Flutax-2 plus 1% Me_2SO (*dotted line*) were added and manually mixed into the solution. Measurements were accumulated for 15 min, starting 5 min after the additions. *B* (*curve a*), time course of the taxoid-induced change in position of the J_{01} x-ray scattering maxima of microtubules. A solution of assembled microtubules (67 μM GTP-tubulin in glycerol assembly buffer containing 7 mM $MgCl_2$, 37 °C) was supplemented at time 0 with Flutax-2 (70 μM, 2.5% residual Me_2SO), employing an isothermal fast mixing device (55). The position of the J_{01} maximum is plotted every 10 s. *B*, control of the experimental noise made by mixing 2.5% Me_2SO into microtubules (50 μM tubulin, 50 μM taxotere) in the same buffer. Note that the control is the same one as in (23), since these experiments are of the same batch as the ones of this work. The *dashed lines* are the best exponential or lineal fits to the data, and the *dotted lines* are the 95% confidence intervals of each fit.

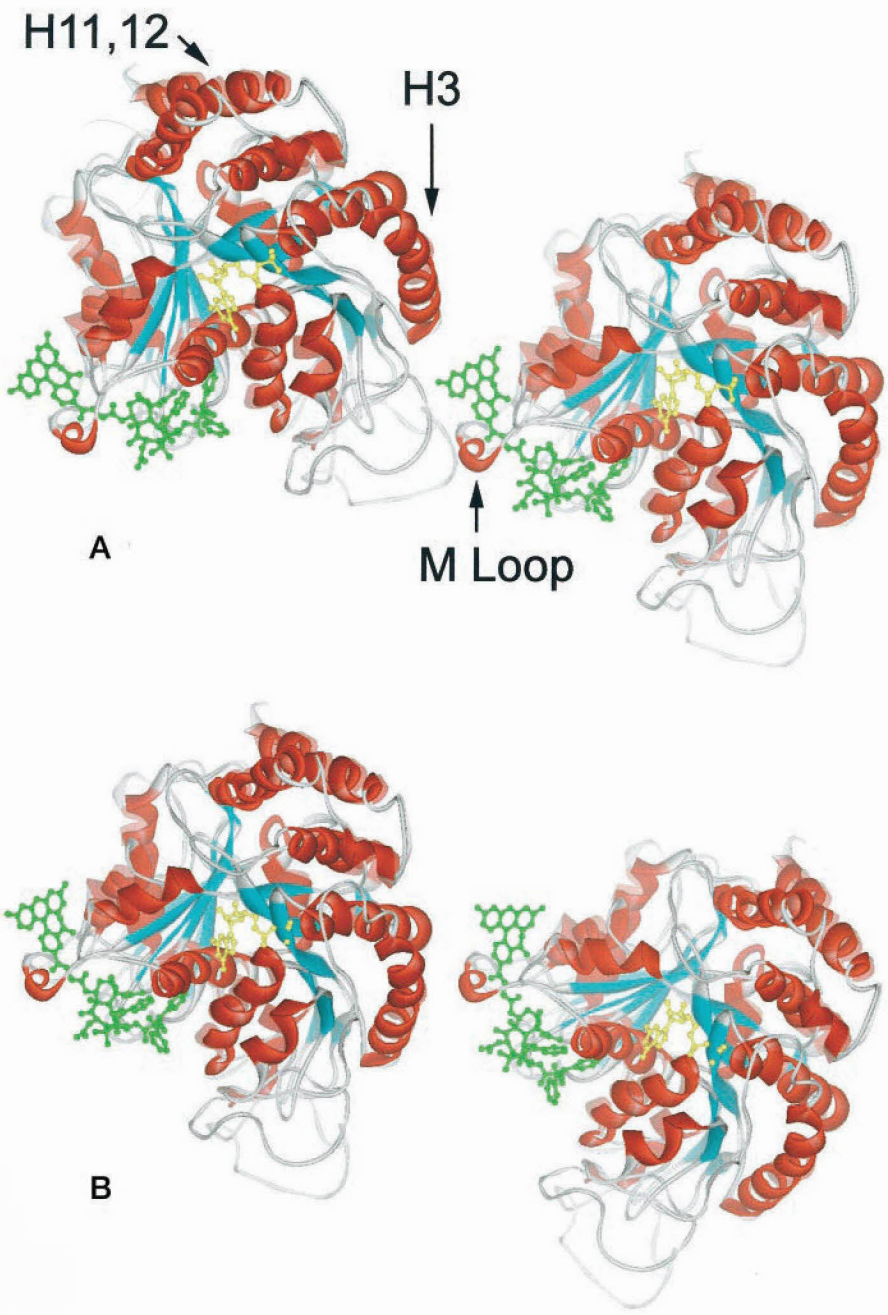

FIG. 10. **Models of the Flutax binding site.** *A*, in the microtubule configuration described by Nogales *et al.* (30). *B*, with the protofilament rotated 30° clockwise as seen from the plus end. The models were constructed by overimposing (using the software package SIMLYS (56)) the taxane moiety of the NMR-determined solution structures of Flutax-1 (57) with the docetaxel molecule modeled in the 1TUB PDB entry (34) and placing the resulting structures either in the same orientation as in Ref. 30 (*A*) or rotated 30° (*B*). Note that the conformation depicted of the bound Flutax-1 is only one of the solution conformations. The fluorescein group has a large conformational freedom with three main orientations, one of them being not allowed for bound Flutax, since it will collide with the protein. From the other two types of configurations, 1) with the fluorescein in the interprotofilament region and 2) with it pointing to the lumen, the first one has been selected, since 1) the internalization of the fluorescein group would be kinetically unfavorable and 2) the dianionic form of the chromophore is stabilized by the positive charge or Arg^{282}. Nevertheless, it is possible that Flutax binds first in configuration 1 and that the second step of binding observed entails flipping to conformation 2.

bules at 37 °C is $1.38 \times 10^6\ M^{-1}\ s^{-1}$; thus, 2.1% of the collisions have to be effective. The problem of the efficiency of collisions has been addressed for protein-protein recognition (49, 50). A typical factor between frequency of collisions and frequency of binding is about 1/1000 and lower for protein-protein interactions. This value holds on the percentage of the surface area of the proteins that forms the binding interface (typically 10% of the exposed area) and other factors like electrostatic or hydrophobic interactions. The value of 1/50 can be a possible ratio for an exposed site in the microtubule. The interface area of Flutax can be roughly estimated in 25% of its total surface by superimposing the taxane moiety of Flutax with the docetaxel molecule bound to tubulin (34). The percentage of interface area of tubulin is also increased (with respect to unassembled protein), since the exposed area of β-tubulin available for collision with ligand is largely reduced in the microtubules, thus increasing the chances of an effective collision.

In this way, mechanism 1 is the easiest possible explanation for the kinetic data. This is supported as well by preliminary results which show that the presence of microtubule-associated proteins, which bind to the outer microtubule surface, slows down the binding of Taxol.[4] Mechanisms of type 1 are in contrast with the location of the Taxol site in the high resolution model microtubules (30), which shows the Taxol site clearly facing the lumen, thus reducing its accessibility.

Let us consider the alternative mechanisms of type 4; Taxol may reach the binding site by diffusing though the microtubule wall. It can be shown that in order to feed the binding reaction at the observed association rate, the effective viscosity of the microtubule wall has to be only 100 times larger than that of water (*i.e.* approximately the viscosity of glycerol), which is highly unreasonable for a protein. Therefore, holes in the microtubule wall would be required. Following the high resolution

[4] J. F. Díaz and J. M. Andreu, unpublished observations.

model of microtubules (30) and recent three-dimensional reconstruction of electron microscopy (51), there are fenestrations in the microtubule wall of roughly 1 nm diameter. Nogales *et al.* (30) suggested that Flutax-1 may pass through the fenestrations to explain the rapid labeling observed by Evangelio *et al.* (24). The Taxol molecule has ellipsoidal axes of 1.7 × 1.5 × 1.5 nm, so it would hardly fit through a 1-nm channel. Flutax-1 and Flutax-2 have a larger size, 2.8 × 1.7 × 1.4 nm in their extended configuration, and it may be impossible for them to pass through such a hole. Nevertheless, let us consider the hypothesis that the real size of the pores could be large enough (say 2.5-nm diameter) to allow ligand diffusion through them and calculate how such a process would influence the kinetics of the binding reaction. Having a pore of 2.5-nm diameter and 3-nm depth (the size of the pore in the model of Nogales *et al.* (30) is about 1.6 × 0.8 nm with 3-nm depth), a molecule of 2-nm diameter will have only 0.82% of the microtubule surface available to collide with it, and only 5.29% of the collisions will have the right angle to pass through the pore. This means that roughly only 1 of every 2300 collisions will transport the ligand inside the lumen, still less than necessary (1 of 50) to feed the reaction. Therefore, the flux of ligand would not be fast enough to feed the binding reaction even if once the ligand is inside the lumen the reaction is purely diffusion-controlled. This combined with the fact that the fenestrations in the MT models are smaller than the ligand makes this mechanism improbable.

A second previously suggested possible mechanism of type 4 (23, 30) would be one in which microtubules would be completely opened in certain parts. It is evident that this would not be a static situation. A kind of microtubule breathing should exist; otherwise, a part of the sites would be freely accessible (those close to the openings), and the ligand access to other sites would need to diffuse from the open parts to the closed parts giving heterogeneous kinetics (the case for the parts far away from the openings would be equivalent, then, to diffusion from the microtubule ends (24)). This possibility can be excluded, since cross-linking of microtubules should extinguish the breathing, resulting in microtubules with two types of sites, the accessible and the inaccessible, thus giving heterogeneous kinetics as discussed above. This was not the case, since cross-linking affected neither the mechanism nor the observed kinetic rates.

A third type of mechanism that may be considered is one of an allosteric type, in which microtubules would have many binding sites, only a few of them being accessible. Taxol binding would alter the geometry of the tubulin molecule, giving access to the other sites. This would be supported by the known fact that binding of taxoids alters the structure of the microtubules (Ref. 23 and this work). However, with such a type of mechanism, the observable kinetic curve cannot be expressed by a single exponential, since the concentration of accessible sites is not constant during the reaction unless each taxoid bound gives access only to the next site, making the observed rate constant dependent on the initial concentration of accessible sites. This is not the case, since cross-linking of the microtubules does not affect the kinetics of the binding reaction, which should have been modified, since cross-linking reduces the conformational freedom of the microtubule.

In summary, we found no feasible explanation of how Taxol might get through the microtubule wall in order to bind so rapidly to a site in the lumen, and retract from such previous discussions (23) in view of the present results. Therefore, we propose that the Taxol binding site has to be at the same reaction compartment as the bulk solution, *i.e.* accessible at the microtubule surface.

Possible Location of the Taxol Binding Site and Consequences for Microtubule Structure—The location of Taxol at the microtubule lumen in the high resolution model of microtubule (30) is in contradiction with the measured kinetic data and the above discussion. Nevertheless, let us point out that the three-dimensional model of tubulin structure (34) is not incompatible with the kinetic data; only the three-dimensional model of microtubules obtained by fitting the tubulin structure into a microtubule electron microscopy density map (30) is apparently contradictory with the data. How would it be possible to reconcile the experimental results of this work with the well supported position of the binding site in a defined zone of β-tubulin (31–33, 52, 53)?

A useful hint is provided by the results with a benzophenone derivative of Taxol at nonessential position 7 (33) (the same position as Flutax), which labels β-tubulin Arg^{282} at the M loop, thus pointing from the inner zones of binding of the essential side chain at position 13 and benzoyl group at position 2 toward the interprotofilament zone. A model similar to that of Nogales *et al.* (30) has been constructed, in which the taxane moiety of Flutax-1 is superimposed with the docetaxel molecule (Fig. 10*A*). Interestingly, this superposition places the ionizable proton of fluorescein close to Arg^{282}, whose positive charge should displace the ionization equilibrium of the fluorescein chromophore toward the dianionic form, as observed experimentally. Then the tubulin dimers have been rotated clockwise (as seen from the plus end of the microtubule) in 5° steps. A rotation of 30–45° is enough to generate a model in which the taxoid binding site is in the interprotofilament area, accessible to the drug from the outside (Fig. 10*B*). It has to be pointed out that the cross-correlation coefficient used to dock the structure of tubulin into microtubules (Fig. 1; Ref. 30) shows a broad peak around the best fitting position, allowing in principle a certain rotational freedom for suboptimal fitting. Second, the parts that may produce steric conflicts if rotated are loops difficult to trace at the resolution of the structure (3.7 Å) and that do not need to have the same structure in Zn^{2+}-induced sheets and microtubules, which have in addition different interprotofilament contacts. So in principle it is possible to consider alternative microtubule models in which the protofilament is rotated or its structure modified in a presently unknown manner, so the taxol site is exposed.

We have analyzed the compatibility of both types of microtubule model with the surface mapping of the tubulin dimer and Taxol-induced microtubules obtained with limited proteolysis (54). Contradictions include the following. 1) The proteolytic sites α(Glu^{290}-Ile^{291}) and α(Ala^{294}-Cys^{295}) are accessible in Taxol microtubules (54). In the model of Nogales *et al.* (30) (Fig. 10*A*), these residues are in the interprotofilament space forbidden to proteases, while in the rotated model (Fig. 10*B*) they lie in the outer surface. 2) The proteolysis sites α(Lys^{280}-Ala^{281}) and β(Tyr^{281}-Arg^{282}-Ala^{283}), both in the M loop (flanking the Taxol binding site), are accessible in tubulin dimers and protected in microtubules (54). In the high resolution model (30), those residues (and thus the Taxol binding site) are accessible at the lumen of the microtubule (proteases should be able to diffuse through the lumen in the 20 min of incubation time employed). In the rotated models, those residues lie between the protofilaments, being inaccessible.

A microtubule structure such as in the rotated protofilament model (Fig. 10*B*) would allow a fast kinetic binding and dissociation of taxoids while keeping the mapped position of the Taxol binding site at the β-tubulin subunit (30). In fact, the location of Taxol in the interprotofilament space has been proposed on structural (26), thermodynamic (14), and assembly kinetic results (20, 23). It is consistent with the perturbing effects of modifications of the taxoid side chain (27) and at

position 7 (this work) on the curvature of the microtubule wall. A rotated protofilament model (Fig. 10*B*) has important structural implications for the mainly electrostatic interprotofilament interactions and the interaction with motor proteins. The M loop (30) is displaced outwards and makes a closer approach to helix H3 (displaced inwards) instead of the H1-S2 loop of the neighboring subunit. In addition, the C-terminal helices H11 and H12 are displaced and should engage in modified interactions with the microtubule binding sites of kinesin motors (51). Experimental distinction between the two types of models (Fig. 10, *A* and *B*) with direct low resolution structural methods is difficult. However, locating the fluorescein moiety of Flutax at the outer microtubule surface would strongly favor the rotated model. This problem may be addressed by employing macromolecular fluorescence quenchers, antifluorescein antibodies, and perturbants of the binding kinetics.

Acknowledgments—We thank Dr. Francisco Amat-Guerri and Dr. Ulises Acuña for continued support with the synthesis of fluorescent taxoids and useful clarifying discussions, Dr. Pilar Lillo for help with the use of the SLM-8000 fluorometer, Dr. Juan Evangelio for initial help with the fluorescent probes, Dr. Consuelo López for use of the stopped-flow apparatus, Dr. Greg Diakun and Dr. Pablo Chacón for help with small angle x-ray scattering measurements, Dr. P. Huitorel for the axonemes, and Aurelio Hurtado and Lorenzo Alonso (CIB Technical Services) for helping with the design and manufacturing of the manual mixing device.

REFERENCES

1. Jordan, A., Hadfield, J. A., Lawrence, N. J., and McGown, A. T. (1998) *Med. Res. Rev.* **18,** 259–296
2. Shi, Q., Chen, K., Morris-Natschke, S. L., and Lee, K. H. (1998) *Curr. Pharm. Des.* **4,** 219–248
3. McGuire, W. P., Brady, M. F., and Ozols, R. F. (1999) *Ann. Oncol.* **10,** (suppl.) 29–34
4. Gelmon, K., Eisenhauer, E., Bryce, C., Tolcher, A., Mayer, L., Tomlinson, E., Zee, B., Blackstein, M., Tomiak, E., Yau, J., Batist, G., Fisher, B., and Iglesias, J. (1999) *J. Clin. Oncol.* **17,** 3038–3047
5. Rowinsky, E. K. (1997) *Semin. Oncol.* **24,** Suppl. 19, 1–12
6. Yvon, A. M., Wadsworth, P., and Jordan, M. A. (1999) *Mol. Biol. Cell* **10,** 947–959
7. Menéndez, M., Rivas, G., Díaz, J. F., and Andreu, J. M. (1998) *J. Biol. Chem.* **273,** 167–176
8. Díaz, J. F., Pantos, E., Bordas, J., and Andreu, J. M. (1994) *J. Mol. Biol.* **238,** 214–225
9. Symmons, M. F., Martin, S. R., and Bayley, P. M. (1996) *J. Cell Sci.* **109,** 2755–2766
10. Díaz, J. F., and Andreu, J. M. (1993) *Biochemistry* **32,** 2747–2755
11. Schiff, P. B., Fant, J., and Horwitz, S. B. (1979) *Nature* **277,** 665–667
12. Parness, J., and Horwitz, S. B. (1981) *J. Cell Biol.* **91,** 479–487
13. Carlier, M. F., and Pantaloni, D. (1983) *Biochemistry* **22,** 4814–4822
14. Díaz, J. F., Menéndez, M., and Andreu, J. M. (1993) *Biochemistry* **32,** 10067–10077
15. Kumar, N. (1981) *J. Biol. Chem.* **256,** 10435–10441
16. Schiff, P. B., and Horwitz, S. B. (1981) *Biochemistry* **20,** 3247–3252
17. Parness, J., Asnes, C. F., and Horwitz, S. B. (1983) *Cell Motil. Cytoskeleton* **3,** 123–130
18. Choudhury, G. G., Bhattacharyya, B., and Biswas, B. B. (1987) *Biochem. Cell Biol.* **65,** 558–564
19. Caplow, M., Shanks, J., and Ruhlen, R. (1994) *J. Biol. Chem.* **269,** 23399–23402
20. Díaz, J. F., Andreu, J. M., Diakun, G., Towns-Andrews, E., and Bordas, J. (1996) *Biophys J.* **70,** 2408–2420
21. Han, Y., Chaudhary, A. G., Chordia, M. D., Sackett, D. L., Perez-Ramirez, B., Kingston, D. G., and Bane, S. (1996) *Biochemistry* **35,** 14173–14183
22. Vulevic, B., and Correia, J. J. (1997) *Biophys. J.* **72,** 1357–1375
23. Díaz, J. F., Valpuesta, J. M., Chacón, P., Diakun, G., and Andreu, J. M. (1998) *J. Biol. Chem.* **273,** 33803–33810
24. Evangelio, J. A., Abal, M., Barasoain, I., Souto, A. A., Lillo, M. P., Acuña, A. U., Amat-Guerri, F., and Andreu, J. M., (1998) *Cell Motil. Cytoskeleton* **39,** 73–90
25. Li, Y., Edsall, R., Jr., Jagtap, P. G., Kingston, D. G. I., and Bane, S. (2000) *Biochemistry* **39,** 616–623
26. Andreu, J. M., Bordas, J., Díaz, J. F., Garcia de Ancos, J., Gil, R, Medrano, F. J., Nogales, E., Pantos, E., and Towns-Andrews, E. (1992) *J. Mol. Biol.* **226,** 169–184
27. Andreu, J. M., Díaz, J. F., Gil, R., de Pereda, J. M., Garcia de Lacoba, M., Peyrot, V., Briand, C., Towns-Andrews, E., and Bordas, J. (1994) *J. Biol. Chem.* **269,** 31785–31792
28. Dye, R. B., Fink, S. P., and Williams, R. C., Jr. (1993) *J. Biol. Chem.* **268,** 6847–6850
29. Nogales, E., Wolf, S. G., Khan, I. A., Ludueña, R. F., Downing, K. H. (1995) *Nature* **375,** 424–427
30. Nogales, E., Whittaker, M., Milligan, R. A., and Downing, K. H. (1999) *Cell* **96,** 79–88
31. Rao, S., Orr, G. A., Chaudhary, A. G., Kingston, D. G. I., and Horwitz, S. B. (1995) *J. Biol. Chem.* **270,** 20235–20238
32. Gonzalez-Garay, M. L., Chang, L., Blade, K., Menick, D. R., and Cabral, F. (1999) *J. Biol. Chem.* **274,** 23875–23882
33. Rao, S., He, L., Chakravarty, S., Ojima, I., Orr, G. A., and Horwitz, S. B. (1999) *J. Biol. Chem.* **274,** 37990–37994
34. Nogales, E., Wolf, S. G., and Downing, K. (1998) *Nature* **391,** 199–203
35. Souto, A. A., Acuña, A. U. Andreu, J. M., Barasoain, I. Abal, M., and Amat-Guerri, F. (1995) *Angew. Chem. Int. Ed. Engl.* **34,** 2710–2712
36. Bevington, P. R. (1969) *Data Reduction and Error Analysis for the Physical Sciences*, pp. 235–240, McGraw-Hill Book Co., New York
37. Peterman, B. F. (1979) *Anal. Biochem.* **93,** 442–444
38. Barshop, B. A., Wrenn, R. F., and Frieden, C. (1983) *Anal. Biochem.* **130,** 134–145
39. Scheele, R. B., Bergen, L. G., and Borisy, G. G. (1982) *J. Mol. Biol.* **154,** 485–500
40. Evans, L., Mitchinson, T., and Kirschner, M. (1985) *J. Cell Biol.* **100,** 1185–1191
41. Oosawa, F., and Asakura, S. (1975) *Thermodynamics of the Polymerization of Protein*, pp. 204, Academic Press, London
42. Lee, J. C., and Timasheff, S. N. (1975) *Biochemistry* **14,** 5183–5187
43. Lee, J. C., and Timasheff, S. N. (1977) *Biochemistry* **16,** 1754–1764
44. Prakash, V., and Timasheff, S. N., (1982) *J. Mol. Biol.* **160,** 499–515
45. Himes, R. H., Jordan, M. A., and Wilson, L. (1982) *Cell Biol. Int. Rep.* **6,** 667–704
46. Cross, A. R., and Williams, R. C., Jr. (1991) *Cell Motil. Cytoskeleton* **20,** 272–278
47. Turner, D., Chang, C., Fang, K., Cuomo, P., and Murphy, D. (1996) *Anal. Biochem.* **242,** 20–25
48. Berg, H. C. (1983) *Random walk in Biology*, pp 17–36, Princeton University Press, Princeton, NJ
49. Northrup, S. H., and Erickson, H. P. (1992) *Proc. Natl. Acad. Sci. U. S. A.* **89,** 3338–3342
50. Janin, J. (1997) *Proteins Struct. Funct. Genet.* **28,** 153–161
51. Kikkawa, M., Okada, Y., and Hirokawa, N. (2000) *Cell* **100,** 241–252
52. Giannakakou, P., Sackett, D. L., Kang, Y. K., Zhan, Z., Buters, J. T., Fojo, T., and Poruchynsky, M. S. (1997) *J. Biol. Chem.* **272,** 17118–17125
53. Monzó, M., Rosell, R., Sánchez, J. J., Lee, J. S., O'Brate, A., González-Larriba, J. L., Alberola, V., Lorenzo, J. C., Núñez, L., Ro, J. Y., and Martín, C. (1999) *J. Clin. Oncol.* **17,** 1786–1793
54. De Pereda, J. M., and Andreu, J. M. (1996) *Biochemistry* **35,** 14184–14202
55. Díaz, J. F., Strobbe, R., Engelborghs, Y., Chacón, P., Andreu, J. M., and Diakun, G. (1998) *Rev. Sci. Instrum.* **69,** 286–289
56. Krüger, P., Lüke, M., and Szameit, A. (1991) *Computer Physics Commununi-cations* **62,** 371–380
57. Jiménez-Barbero, J., Souto, A. A., Abal, M., Barasoain, I., Evangelio, J. A., Acuña, A. U., Andreu, J. M., and Amat-Guerri, F. (1998) *Bioorg. Med. Chem.* **6,** 1857–1863
58. Souto, A. A. (1997) *Síntesis, caracterización, y aplicaciones de nuevas soudas fluorescentes, para membranas y proteínas. Acidos peutaenoicos conjugados y derivados de taxol*. Ph.D. thesis, Universidad Complutense de Madrid

Molecular Recognition of Taxol by Microtubules: KINETICS AND THERMODYNAMICS OF BINDING OF FLUORESCENT TAXOL DERIVATIVES TO AN EXPOSED SITE

J. Fernando Di?az, Rik Strobe, Yves Engelborghs, André A. Souto and José M. Andreu

J. Biol. Chem. 2000, 275:26265-26276.
doi: 10.1074/jbc.M003120200 originally published online May 18, 2000
